Monthly Notices
of the
ROYAL ASTRONOMICAL SOCIETY

MNRAS **493,** 3947–3955 (2020)
Advance Access publication 2020 February 20

doi:10.1093/mnras/staa489

Molecular environments of the supernova remnant G359.1−0.5

L. K. Eppens,[1,2★] E. M. Reynoso,[1★] J. Lazendic-Galloway,[3] J. A. Combi[2,4] and J. F. Albacete-Colombo[5]

[1]*Instituto de Astronomía y Física del Espacio, CONICET-UBA, Buenos Aires, Argentina*
[2]*Facultad de Ciencias Astronómicas y Geofísicas, Universidad Nacional de La Plata, La Plata, Buenos Aires, Argentina*
[3]*School of Physics and Astronomy, Monash University, Clayton VIC 3800, Australia*
[4]*Instituto Argentino de Radioastronomía, CONICET – CICPBA, Argentina, Buenos Aires, Argentina*
[5]*Universidad Nacional de Rio Negro, Sede Atlántica – CONICET, Viedma CP8500, Río Negro, Argentina*

Accepted 2020 February 14. Received 2020 February 3; in original form 2020 January 7

ABSTRACT

We report new CO observations and a detailed molecular-line study of the mixed morphology supernova remnant G359.1−0.5, which contains six OH (1720 MHz) masers along the radio shell, indicative of shock-cloud interaction. Observations of ^{12}CO and ^{13}CO J:1–0 lines were performed in a ∼38 × 38 arcmin area with the on-the-fly technique using the Kit Peak 12 Meter telescope. The molecular study has revealed the existence of a few clumps with densities $\sim 10^3$ cm^{-3} compatible in velocity and position with the OH (1720 MHz) masers. These clumps, in turn, appear to be part of a larger, elongated molecular structure ∼34 arcmin long extending between −12.48 and +1.83 km s^{-1}, adjacent to the western edge of the radio shell. According to the densities and relative position with respect to the masers, we conclude that the CO clouds depict unshocked gas, as observed in other remnants with OH (1720 MHz) masers. In addition, we investigated the distribution of the molecular gas towards the adjacent γ-ray source HESS J1745-303 (Aharonian et al. 2006) but could not find any morphological correlation between the γ-rays and the CO emission at any velocity in this region.

Key words: ISM: clouds – ISM: individual: (G359.1−0.5) – ISM: molecules – ISM: supernova remnant.

1 INTRODUCTION

Core-collapse supernova (SN) explosions are the final stage in the evolution of high mass stars (≥8 M$_\odot$). These events produce a diffuse component and a compact object (neutron star or black hole). The diffuse component, called supernova remnant (SNR), results from the combination of the leftover stellar material and the interstellar gas swept up by the shock wave driven by the SN outburst. The expanding shock wave creates a shell morphology that radiates non-thermal emission in radio band (sometimes observed in X-rays as well), created from electrons accelerated in magnetic field from the compressed interestellar medium (ISM). At the same time, the expanding shock carries ejected hot stellar material and heats the swept up ISM, and these two components can be detected in the X-ray band as thermal emission. However, there is a fraction of SNRs for which the X-ray emission, rather than forming a shell, fills the centre of the radio remnants, creating a separate morphological group named mixed-morphology (MM) SNRs (Rho & Petre 1998). The galactic source G359.1−0.5 belongs to this group of remnants.

G359.1−0.5 was initially detected by Altenhoff et al. (1979) in a Galactic Plane survey at 4.9 GHz. A flux density of ∼13 Jy was estimated. Subsequent observations at 2.7 GHz and 4.8 GHz (Reich & Fuerst 1984) classified it as a shell-type SNR based on the non-thermal spectrum ($\alpha = -0.37$) and polarized emission (11.5 per cent).

There are three X-ray studies that reveal the thermal nature of the filling plasma inside G359.1−0.5. In the first one, Egger & Sun (1998) identified diffusive X-rays with the Röntgensatellit (*ROSAT*) All Sky Survey (RASS; Truemper 1992, 1993) observations, classifying this remnant in the MM group. They fitted the data with a two temperature thermal plasma with the cooler plasma abundant in Silicon (Si), while the hotter component was extremely over-abundant in Sulphur (S). Those results implied that the thermal X-rays emission originated in the ejecta rather than swept up ISM. The second analysis was performed with the Advanced Satellite for Cosmology and Astrophysics by Bamba et al. (2000), where the authors recognized prominent Kα lines of Si and S in the spectrum, which were consistent with He-like and H-like ions, respectively. However, the third X-ray study based on Suzaku observations (Ohnishi et al. 2011) disagreed with the two-component model and proposed an overionized state of the inner plasma. Ohnishi et al. (2011) suggested that the ions are cooling

★ E-mail: leppens@iafe.uba.ar (LKE); ereynoso@iafe.uba.ar (EMR)

faster than electrons, supposedly as a consequence of interaction with a denser environment.

G359.1−0.5 belongs to a group of SNRs that have associated OH (1720 MHz) masers (Green et al. 1997; Frail & Mitchell 1998; Koralesky et al. 1998). These particular masers are tracers of interaction between SNRs and molecular gas, since they are excited when the shock front hits the surrounding molecular material (Elitzur 1976). Yusef-Zadeh et al. (1995) found six masers strikingly distributed along the edge of G359.1−0.5 with velocities between $-5.57 < v < -2.9$ km s^{-1}. They discarded that the 1720-MHz line emission had origin in spiral arms foreground dark clouds (e.g. Turner 1982), which amplify background radiation, since no continuum emission is detected at the locations of masers B and D, while regions of brighter continuum emission over the shell or even beyond do not coincide with any 1720-MHz line emission spot. Also, the fact that no masers are found in the interior but all of them are on the outer shell, together with an extended 1720-MHz component that closely follows the edge of the remnant (see Section 4.1) strongly suggests that shocks are involved. Based on all this evidence, they proposed that the OH (1720 MHz) masers are being generated behind the shock front and, therefore, are associated with the SNR.

Uchida et al. (1992b) inspected the molecular distribution towards G359.1−0.5 in the ^{12}CO J = 1-0 line and found a nearly continuous ring of molecular gas ($-190 < v < -60$ km s^{-1}) coincident with the radio shell. A follow-up study of the H I line using VLA data (Uchida, Morris & Yusef-Zadeh 1992a) shows a counterpart of the CO ring between −190 and −75 km s^{-1}. A simultaneous H I absorption study showed that there were H I features at −60 and −135 km s^{-1} towards G359.1−0.5. However, the subsequent discovery of the OH (1720 MHz) masers at a significantly different velocity casts doubts on the connection between this annular cloud and the SNR. Lazendic et al. (2002) obtained new high-resolution molecular data focusing on a smaller field towards maser A. They found a shocked cloud coincident in position and velocity with the maser.

An extended unidentified γ-ray source, HESS J1745-303, was also detected in the vicinity of G359.1−0.5 (Aharonian et al. 2006). A GeV counterpart to this TeV source was detected with the *Fermi* Large Area Telescope (LAT; Hui et al. 2011). The nature of HESS J1745-303 is still uncertain and its association with G359.1−0.5 remains a matter of debate.

This paper reports original 12 Meter Radio Telescope observations in the ^{12}CO and ^{13}CO J:1–0 lines with an improved resolution as compared to previous surveys covering the full extent of G359.1−0.5 and surroundings. We aim to re-visit the molecular gas distribution around the SNR and confirm or reject the previous claims for CO structures related to it. The outline of the paper is as follows: in Section 2, we describe the molecular line observations and data reduction. The results of the molecular analysis is presented in Section 3. In Section 4, we discuss the implications of our results, including the possible connection between the molecular gas distribution and the origin of the γ-rays emission. Finally, we summarize the main conclusions in Section 5.

2 OBSERVATIONS AND DATA REDUCTION

Observations were performed on 2002 February with the Arizona Radio Observatory 12M Radio Telescope located at Kitt Peak, Arizona. The observed field, covering ∼38 × 38 arcmin, was scanned applying the on-the-fly technique, efficient for imaging extended regions. Two spectrometers centred at −5.0 km s^{-1} were used, both having 256 channels but with different resolutions of 250 and 500 kHz (0.65 and 1.3 km s^{-1}) for the ^{12}CO line and 100 and 500 kHz (0.27 and 1.35 km s^{-1}) for the ^{13}CO. The ^{12}CO line (centred at 115.271204 GHz) was observed during 4.5 h on February 23, while the ^{13}CO (centred at 110.201353 GHz) was observed for 3.25 h on February 24.

Data processing was carried out using the AIPS package. A set of line-free channels was selected for baselines subtraction, which was applied to the whole map through the task 'least squares fit baseline and subtracts from SD data' (SDLSF). The line-free channels selection was aided with an H I spectrum obtained from the Leiden−Argentina–Bonn Survey (Kalberla et al. 2005). Data editing was performed with WIPER and corrupted observations were removed. The data cubes were constructed with the task 'select and grid random-position single-dish measurements' (SDGRD). A few spread channels needed to be fully removed and were replaced by an average between the preceding and subsequent channels. The spatial resolution is 53.6 arcsec × 53.6 arcsec and 56.0 arcsec × 56.0 arcsec for the ^{12}CO and ^{13}CO, respectively.

Table 1. OH (1720 MHz) masers.

Maser	R.A.(J2000)	Dec.(J2000)	V_{LSR} (km s^{-1})	S (mJy)
A	17:44:58.06	− 29:51:03.7	− 4.47	761
B	17:44:42.026	− 29:58:00.49	− 2.9	59.5
C_1	17:44:56.27	− 30:06:00.8	− 3.19	215
C_2	17:44:58.19	− 30:05:47.87	− 5.57	732
D	17:45:44.92	− 30:08:33.4	− 5.28	639
E	17:46:12.96	− 29:55:19.0	− 5.08	93

Note. Names and parameters of the OH (1720 MHz) masers are taken from Yusef-Zadeh et al. (1995)[3].

3 RESULTS

As mentioned above, G359.1−0.5 is one of the SNRs for which OH (1720 MHz) masers were detected. The physical conditions for the collisional excitation of these masers are moderate temperatures ($50 < T < 125$ K) with densities $10^4 \leq n_H \leq 5 \times 10^5$ cm^{-3} and OH column densities of 10^{16}–10^{17} cm^{-2} (Lockett, Gauthier & Elitzur 1999). Frail et al. (1996) noted that masers are more easily detected when the acceleration of the molecular gas produced by the SNR shock is transverse to the line of sight. Hence, the velocity of the OH (1720 MHz) masers is coincident with the systematic velocity of the pre-shock molecular gas, with a very low dispersion around this value.

In Table 1, we reproduce the masers parameters as obtained from Yusef-Zadeh et al. (1995). The first column indicates the name of each maser following the same nomenclature as in their paper. The next two columns list the coordinates converted to J2000.0, including the correction in the declination for maser D (Qiao et al. 2018).[1] These positions are indicated by crosses in Fig. 1 (see below). The fourth column presents the radial velocity for each maser in km s^{-1} and the last one shows the flux density in units of mJy.

To compare the CO distribution with G359.1−0.5, we used a radio continuum image obtained with the Australian Telescope Compact Array at 1.5 GHz (Yusef-Zadeh, Hewitt & Cotton 2004). This image has a resolution of 20.87 arcsec × 18.20 arcsec, P.A.

[1]Qiao et al. (2018) detected a typo error in Yusef-Zadeh et al. (1995). We show the corrected value.

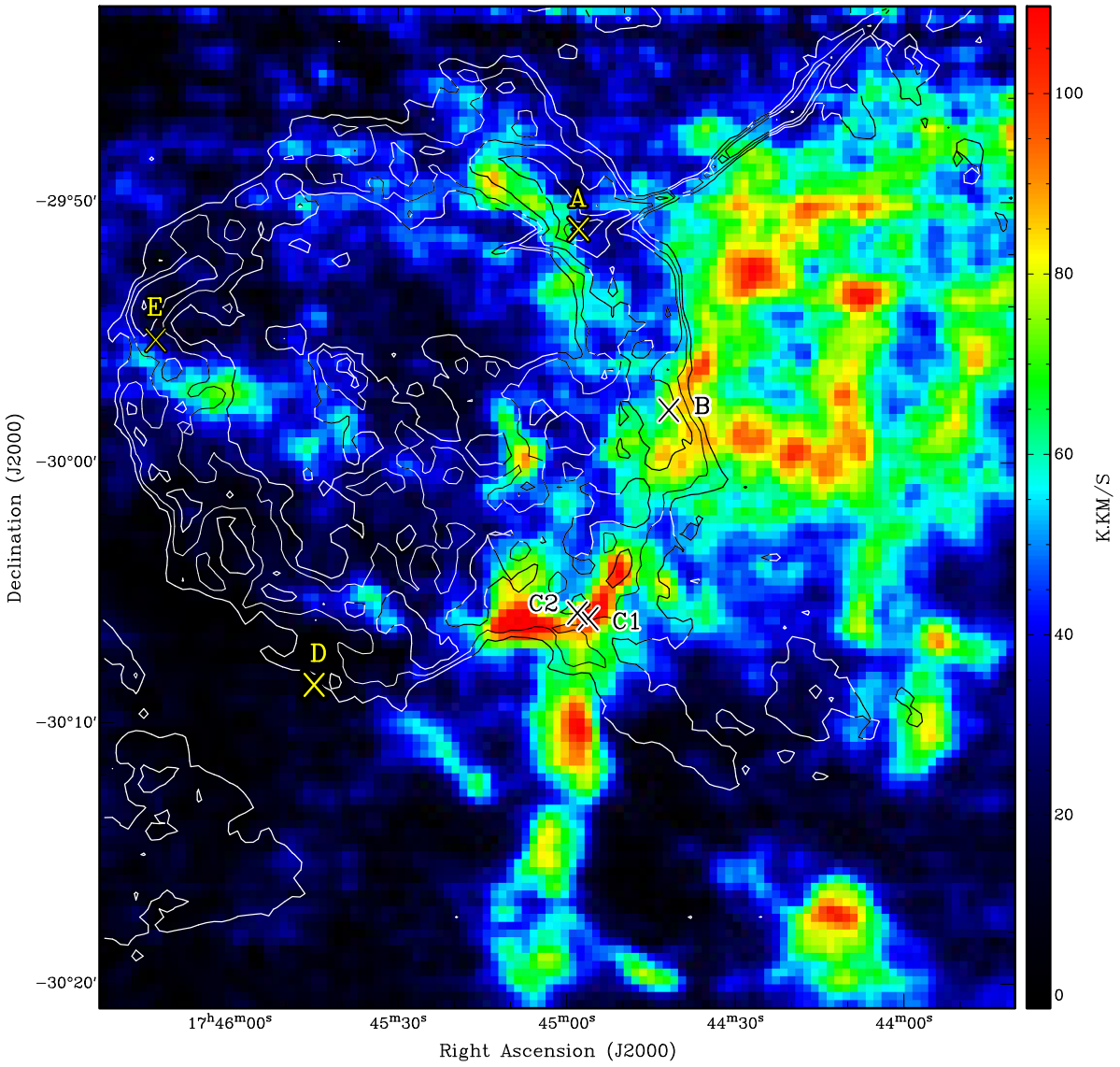

Figure 1. Distribution of ^{12}CO emission integrated between −12.48 and +1.83 km s^{-1}. The beam size is 53.6 arcsec × 53.6 arcsec. The colour scale is indicated at the right in units of K km s^{-1}. Contours (white or black depending on background) at 0.003, 0.005, 0.008, 0.014, 0.019, and 0.025 mJy beam^{-1} represent the radio emission at 1.5 GHz. The crosses indicate the location of the OH (1720 MHz) masers reported in Yusef-Zadeh, Uchida & Roberts (1995) and are labelled following the same nomenclature.

= −180.5. We inspected the CO data cubes throughout the whole velocity range in order to identify molecular gas features that could be coincident in position and velocity with the OH (1720 MHz) masers. For most of the masers, we found small clouds associated with them, which are embedded in an extended structure extending in velocity from −12.48 km s^{-1} to +1.86 km s^{-1}. This feature can be seen in Fig. 1 at the west of G359.1−0.5, where the ^{12}CO emission is integrated over this velocity interval. In the region overlapping the continuum emission, this CO structure follows the curvature of the radio shell and continues to the south as a tail about 10 arcmin long. In what follows, we will describe the individual structures likely to be associated with each OH (1720 MHz) maser.

In Fig. 2, we show in the upper left-hand panel the ^{12}CO cloud, hereafter 'a_1', correlated with maser A. This arc-shaped structure centred at −4.35 km s^{-1} consists of three clumps. The OH (1720 MHz) maser is located at the edge of the middle clump (see upper right-hand panel in Fig. 2), which will be referred to as 'a_2' and is centred at R.A.(J2000) = 17^{h}45^{m}01.^{s}7, Decl.(J2000) = −29°51′3.″9.

The rest of the clouds identified close to the other five masers are shown in Fig. 2. The second row left-hand panel displays the ^{12}CO distribution around maser B integrated from −5.92 to 0.58 km s^{-1}. This figure shows an extended clump, hereafter 'b_1', centred at R.A.(J2000) = 17^{h}44^{m}38.^{s}1, Decl.(J2000) = −29°57′3.″5, which has a ^{13}CO counterpart.

The masers C_1 and C_2 are positionally very close to one another but differ in velocity by more than 2 km s^{-1}. We searched for a CO structure compatible with C_1 and found the cloud enclosed by the contour level of 22.1 K km s^{-1} shown in the lower left-hand panel in Fig. 2. This structure, hereafter 'c_1', is observed both in ^{12}CO and ^{13}CO around ∼−3 km s^{-1} and consists of an ∼2 arcmin long concentration extending N–S with an asymmetric intensity distribution, where the peak is at the south, at R.A.(J2000) = 17^{h}44^{m}49.^{s}1, Decl.(J2000) = −30°07′15.″8. The maser lies somewhat afar from c_1

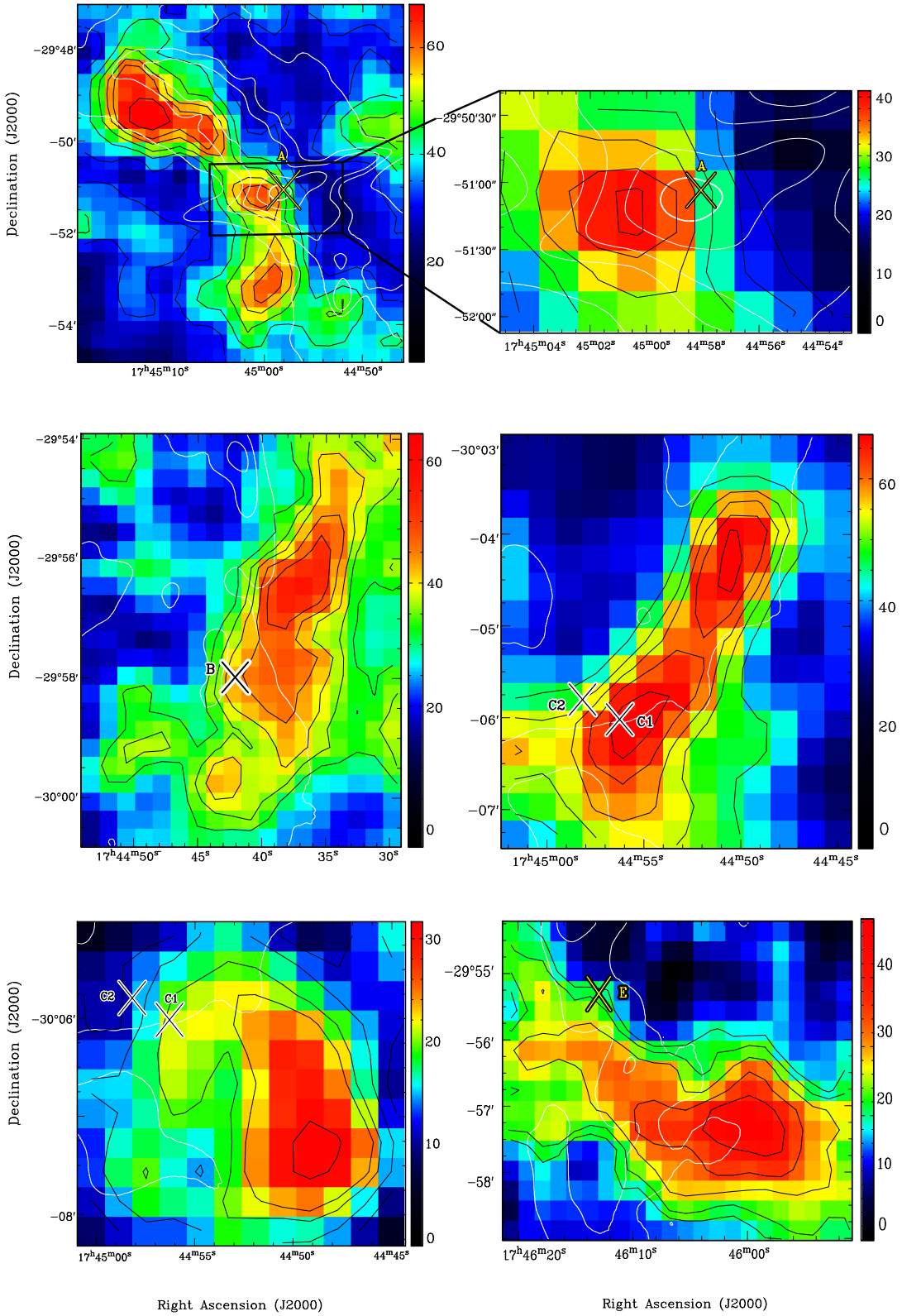

Figure 2. Distribution of ^{12}CO clouds probably associated with each OH (1720 MHz) maser, whose positions are indicated with crosses. The beam size is 53.6 arcsec × 53.6 arcsec. The colour scale is indicated at the right in units of K km s^{-1}, and black contours are overlaid to highlight the detected structures. White contours at 0.003, 0.005, 0.008, 0.014, 0.019, and 0.025 mJy beam^{-1} are used to plot the radio emission at 1.5 GHz. The integration velocity ranges and black contour levels are as follows: Upper left-hand panel : from −8.25 to +0.85 km s^{-1}, levels 32, 41, 47.5, 54.3, 59, and 69 K km s^{-1}. Upper right-hand panel: close-up towards maser A at the same velocities. Middle left-hand panel: from −5.98 to 0.53 km s^{-1}, levels 32, 36, 39.6, 44.2, and 49 K km s^{-1}. Middle right-hand panel: from 3.05 to −8.25 km s^{-1}, levels 45, 52, 56.5, 61.5, and 67 K km s^{-1}. Lower left-hand panel: from −3.5 to −2.42 km s^{-1}, levels 11, 14.8, 19.2, 22.1, and 31.8 K km s^{-1}. Lower right-hand panel: from −7.93 to −2.07 km s^{-1}, levels 19, 22, 27, 33.8, and 41 K km s^{-1}.

Table 2. Physical parameters of CO clumps.

Parameters	a_1	a_2	b_1	c_1	c_2	e_1
RA(J2000) (h m s)	17 45 3.1	17 45 1.7	17 44 38.1	17 44 49.1	17 44 51.9	17 46 2.6
Decl.(J2000) (° ′ ″)	−29 50 10.01	−29 51 3.9	−29 57 3.5	−30 07 15.8	−30 05 9.8	−29 57 21.9
v_i,v_f(^{12}CO) (km s^{-1})	0.85,−8.25	0.85,−8.25	0.53,−5.98	−1.42,−4.67	−3.05,−8.25	−2.07,−7.93
v_i,v_f(^{13}CO) (km s^{-1})	–	–	0.58,−5.45	−2.42,−3.5	–	−2.14,−7.86
T_{peak}(^{12}CO) (K)	10.5	9.8	11.3	13.3	16.4	10.7
T_{peak}(^{13}CO) (K)	–	–	3.9	4.6	–	4.3
T_{exc} (K)	–	–	14.7	16.7	–	14.1
τ(^{13}CO)	–	–	0.43	0.42	–	0.51
N(^{13}CO) (10^{15} cm^{-2})	–	–	32.6	6.8	–	31.5
N_{H_2} (10^{21} cm^{-2})	8.3	5.7	16.3	3.4	10.2	15.7
M_{H_2} ($(\frac{d}{3.7})^2$M$_\odot$)	∼3080	∼190	∼955	∼145	∼690	∼2340
n_{H_2}($\frac{3.7}{d}10^3$ cm^{-3})	∼1.8	∼2.1	∼13.8	∼1.1	∼5.6	∼4.5

Note. Physical parameters for CO clumps associated with the OH (1720 MHz) masers. The velocities v_i and v_f, in units of km s^{-1}, indicate the integration range. The mass M_{H_2} and the volume density n_{H_2} are scaled with the distance in units of kpc.

at the edge of a weak ∼1 arcmin protrusion with no ^{13}CO counterpart that extends to the SE from the northern extreme.

In order to identify the molecular gas associated with maser C_2, we inspected the CO cubes at velocities close to −5.6 km s^{-1} and found the ^{12}CO structure displayed in the right-hand panel at the second row in Fig. 2. This elongated cloud, only detected in ^{12}CO, has two peaks at the extremes. The peak closest to maser C_2 is centred at R.A.(J2000) = 17^{h}44^{m}51^s.9, Decl.(J2000) = −30°05′9″.8 and we will name it 'c_2'.

The lower right-hand panel in Fig. 2 shows a ^{12}CO concentration integrated from −2.07 to −7.93 km s^{-1}, being maser E located outside the northern limit of the cloud. This structure extends along ∼7 arcmin and has a counterpart in the ^{13}CO line. The cloud peak is centred at R.A.(J2000) = 17^{h}46^{m}2^s.6, Decl.(J2000) = −29° 57′21″.9 and we will call it 'e_1'. Maser D is one of the most intense of the OH (1720 MHz) masers reported by Yusef-Zadeh et al. (1995). However, we did not find any molecular emission in its boundaries throughout the whole velocity range observed.

To estimate the masses of the clumps mentioned above, we assumed local thermodynamic equilibrium. We integrated the H_2 column density (N_{H_2}) over the solid angle (Ω) subtended by each CO emission feature and assumed that the molecular gas is at the same distance as G359.1−0.5. The distance to the SNR is not well constrained. While Galactic rotation models are not accurate towards this direction of the Galaxy, there are suggestions that the SNR is at the distance of the Galactic Centre, 8.5 kpc, based on the comparison with X-ray sources with similar absorbing column densities (e.g. Ohnishi et al. 2011). Yusef-Zadeh et al. (1995) sets this distance as an upper limit, since otherwise the SNR diameter would be unrealistically large. We will use the reddening-distance model of Chen et al. (1999) to obtain a new, independent estimation. The details on the application of this method are as in Reynoso, Cichowolski & Walsh (2017). The reddening E(B-V) is derived from the hydrogen column density N_H obtained by measuring the X-ray extinction, estimated to be 2×10^{22} cm^{-2} (Ohnishi et al. 2011). This gives E(B-V) = 2.9 mag. The total reddening produced by the Galactic Plane in the direction of G359.1−0.5 up to the edge of the Galaxy is E(B-V)$_\infty$ = 13.3 ± 1.3 mag (Schlafly & Finkbeiner 2011).[2] Assuming a scale height absorbing dust of 117.7 ± 4.7 pc for the Galactic Plane (Kos et al. 2014) and a distance of 19.6 ± 2.1 pc from the Galactic Plane to the Sun (Reed 2006), the model of Chen et al. (1999) produces a distance of 3.7 ± 0.8 kpc for G359.1−0.5. At this distance, the SNR diameter is estimated to be ∼25 pc, much more reliable that the 60-pc diameter that the remnant would have at the Galactic Centre distance. Nevertheless, we express our final results in terms of d (see Table 2) to facilitate comparison with the results when other distances are assumed.

The ^{13}CO column density can be computed using

$$N\,(^{13}\mathrm{CO}) \;=\; 2.42 \times 10^{14}\;\tau(^{13}\mathrm{CO})\;\frac{\Delta v\;T_{\mathrm{exc}}}{1-\mathrm{e}^{-5.29/T_{\mathrm{exc}}}}\;[\mathrm{cm}^{-2}], \qquad (1)$$

where Δv is the full width at half-maximum (FWHM) line width in units of km s^{-1}, T_{exc}, is the excitation temperature of the $J = 1 \rightarrow 0$ transition of the ^{13}CO molecule in units of K and τ(^{13}CO) is the optical depth given by

$$\tau\,(^{13}\mathrm{CO}) \;=\; -\ln\left(1-\frac{T_{\mathrm{peak}}\,(^{13}\mathrm{CO})}{5.29\;[(\mathrm{e}^{5.29/T_{\mathrm{exc}}}-1)^{-1}-0.164]}\right). \qquad (2)$$

The excitation temperature was estimated by observing the peak temperature of the optically thick CO ($J = 1 \rightarrow 0$) emission and following the equation:

$$T_{\mathrm{exc}} \;=\; \frac{5.53}{\ln[1+5.53/(T_{\mathrm{peak}}(^{12}\mathrm{CO})+0.819)]}\;[\mathrm{K}]. \qquad (3)$$

The N_{H_2} of the clumps is directly derived from the fractional abundance $N_{H_2}/N(^{13}\mathrm{CO}) = 5 \times 10^5$ (Dickman 1978).

Then, the molecular mass of H_2 can be calculated using the formula:

$$M_{H_2} \;=\; \frac{2.72\;m_{\mathrm{H}}}{m_\odot}\;N_{H_2}\;\Omega(^{12}\mathrm{CO})\;d^2\;[\mathrm{M}_\odot], \qquad (4)$$

where we assumed a mean molecular weight per H_2 molecule of 2.72 m_H (Allen 1973), N_{H_2} is in units of cm^{-2}, Ω(^{12}CO) is given in units of str, and d is the distance in units of cm.

For those clouds where only ^{12}CO emission was detected, we calculate N_{H_2} using the relationship $X = N_{H_2}/W_{CO}$, where W_{CO} is the integrated CO line intensity in units of K km s^{-1} and $X = 1.6 \times 10^{20}$ cm^{-2}/K km s^{-1} (Hunter et al. 1997).

Table 2 shows the physical parameters obtained for the CO clumps associated with the OH (1720 MHz) masers, where the names of the clumps are given at the top from column 2 to column 7. The clumps central position (R.A., Decl.) are given in the first two rows. The next two rows show the velocity range where every molecular structure was detected and specify if we found ^{12}CO and/or ^{13}CO emission. Rows 5 and 6 present the ^{12}CO and, if

[2]An online tool for obtaining the dust reddening for a given line of sight is supplied in https://irsa.ipac.caltech.edu/applications/DUST/

applicable, ^{13}CO T_{peak} in units of K obtained from the observations, and row 7 lists T_{exc} in units of K. The calculated parameters $\tau(^{13}CO)$ and $N(^{13}CO)$ in units of cm^{-2} are given in rows 8 and 9. The next row shows N_{H_2} in units of cm^{-2}. Finally, the last two rows display the total mass M_{H_2} in solar masses and the volume density n_{H_2} in units of cm^{-3} for each clump; both parameters are scaled with the distance in units of kpc.

4 DISCUSSION

4.1 CO distribution at the maser velocities

We surveyed the molecular gas towards the OH (1720 MHz) masers and found small cloudlets coincident with most of them both in position and velocity. Only two of the clumps have no ^{13}CO counterpart, probably due to the low density of ^{12}CO which, given that the abundance ratio $N^{12}/N^{13} \sim 20$ (Wilson & Rood 1994), translates into an even lower ^{13}CO density, below the detection limit of our data. The cloudlets are, in turn, embedded within an extended ^{12}CO feature to the west of the SNR radio shell contained in the velocity range $-12.48 < v < 1.86$ km s^{-1}. In some cases, the gas distribution follows closely the curvature of the SNR. For example, at the location of the masers C_1 and C_2, Fig. 1 reveals a bright CO arc that strikingly matches the outer radio contour. A similar trend is observed around masers A and B in Fig. 2. We interpret such remarkable morphological coincidence as an indication of a physical association between the SNR and the molecular gas. Maser E, in contrast, not only does not lie over or very close to any CO cloud but also the nearest cloud cuts the radio contours from east to west rather than following the edge (see Fig. 1). Therefore, we propose that this clump is merely a molecular gas feature not related to the maser or to the remnant itself.

The average difference between the velocities of the OH (1720 MHz) masers and those of the corresponding CO clumps is $\sim$0.12 km s^{-1}, much smaller than the spectral resolution of our data. We can therefore conclude that the clumps are at the same velocity as the OH (1720 MHZ) masers. A major obstacle found by Yusef-Zadeh et al. (1995) to support that the OH (1720) MHz masers originate in G359.1−0.5 was the inconsistency between their velocities and the ambient molecular gas, since they assumed that the molecular cloud associated with the SNR was the CO ring reported by Uchida et al. (1992b) beyond −60 km s^{-1}. Our results sort out this problem.

As regard to the relative position, the distance between each maser and the peak in the CO brightness distribution is typically $\sim$2-3 pc, reaching maser C_1 a distance of 5 pc to the emission peak of the clump c_1. Similar distances were reported between OH (1720 MHz) masers at other SNRs and their corresponding molecular clumps (e.g. Frail & Mitchell 1998; Reynoso & Mangum 2000). The fact that the masers are near but not at exactly the same position of the CO peaks indicates that CO lines at low rotational transitions do not trace regions with density high enough to excite OH (1720 MHz) maser emission. Such density was estimated to be $n_{H_2} \sim 10^5$ cm^{-3} (Lockett et al. 1999). This theoretical prediction was confirmed observationally in several SNRs (e.g. Frail & Mitchell 1998; Brogan et al. 2013).

Lazendic et al. (2002) observed an $\sim 2 \times 2$ arcmin area around maser A in the H_2 1-0 S(1) line and found a linear feature of 1.5-arcmin length and 15-arcsec width containing the maser and lying parallel to the edge of the radio shell. They determined a significant density gradient between the eastern (10^4 cm^{-3}) and western (10^5 cm^{-3}) sides of this feature, supporting the idea that the H_2 originates in the expansion of the shock driven by G359.1−0.5. The H_2 linear feature tightly surrounds clump a_2 to the west (Fig. 2). Based on the relative position and difference in density, we propose that clump a_2 traces the pre-shock gas, while the western edge was compressed by the SNR shock front, attaining the physical conditions necessary to produce amplified maser emission at 1720 MHz. The linear feature was also observed in the CS $J = 3$-2 line (Lazendic et al. 2002), from which an H_2 density of 10^5 cm^{-3} was derived, in coincidence with the values obtained through the H_2 line.

As mentioned in Section 1, Yusef-Zadeh et al. (1995) also found an elongated, weaker maser component that extends about 5 arcmin and appears to link masers A and B. This OH feature spans from −11 to −3 km s^{-1}, with a brightness peak at about −8 km s^{-1}. A comparison with Fig. 2 reveals that the maser emission is placed to the west of the CO emission and stretches beyond the limits of clump a_1. Extended OH (1720 MHz) maser emission is a powerful tracer of shocked gas (Hewitt, Yusef-Zadeh & Wardle 2008).

4.2 CO distribution at other velocities

As mentioned before, Uchida et al. (1992b) described a ^{12}CO structure detected in a $1.^\circ5 \times 1.^\circ5$ field surrounding G359.1−0.5 with an annular morphology concentric with the radio shell and within the velocity range from −190 to −60 km s^{-1}. After the discovery of the five OH (1720 MHz) masers, which provides a strong indication of the systematic velocity of the clouds interacting with SNRs (Frail et al. 1996), the association between the CO ring reported by Uchida et al. (1992b) and G359.1−0.1 can be treated as coincidental. This is not too surprising considering that both molecular clouds and SNRs tend to be circular in shape and chance alignments are very likely. Nevertheless, to investigate the distribution of the clouds at those velocities towards this region, we inspected our ^{12}CO and ^{13}CO data. Fig. 3 shows the CO emission integrated from −60 up to the spectral limit of our observations, −178 km s^{-1}. We observe a structure to the west partially overlapping the radio continuum shell, but we find no evidence of the molecular ring at these velocities.

4.3 Comparison between CO distribution and emission at γ-rays

The γ-ray source HESS J1745-303, adjacent to G359.1−0.5, was first discovered in the High Energy Stereoscopic System (H.E.S.S.) Galactic Plane Survey (Aharonian et al. 2006). This extended TeV complex has been described as consisting of three components (Aharonian et al. 2008). There is growing evidence that region A, the component closer to G359.1−0.5, is unrelated to the other two components (Hui et al. 2011, 2016; de Wilt et al. 2017); hence, we will focus only on this one. In Fig. 4, the TeV emission is represented in blue, while the radio continuum emission is depicted in red and highlighted with white contours, and the CO emission integrated between −12.48 and +1.83 km s^{-1} (see Fig. 1) is represented in green.

Very high-energy γ-rays are basically produced by three mechanisms: (i) up-scatter of lower energy to higher energy photons by interactions with high-energy electrons via the inverse-Compton process, (ii) acceleration of electrons in the electrostatic fields of ions and atomic nuclei via relativistic bremsstrahlung, and (iii) π^0 − decay via interactions of high-energy hadrons (cosmic rays) with the ambient gas. Although the lack of a spectral break in HESS J1745-303 is not compatible with many other GeV-SNRs (Acero

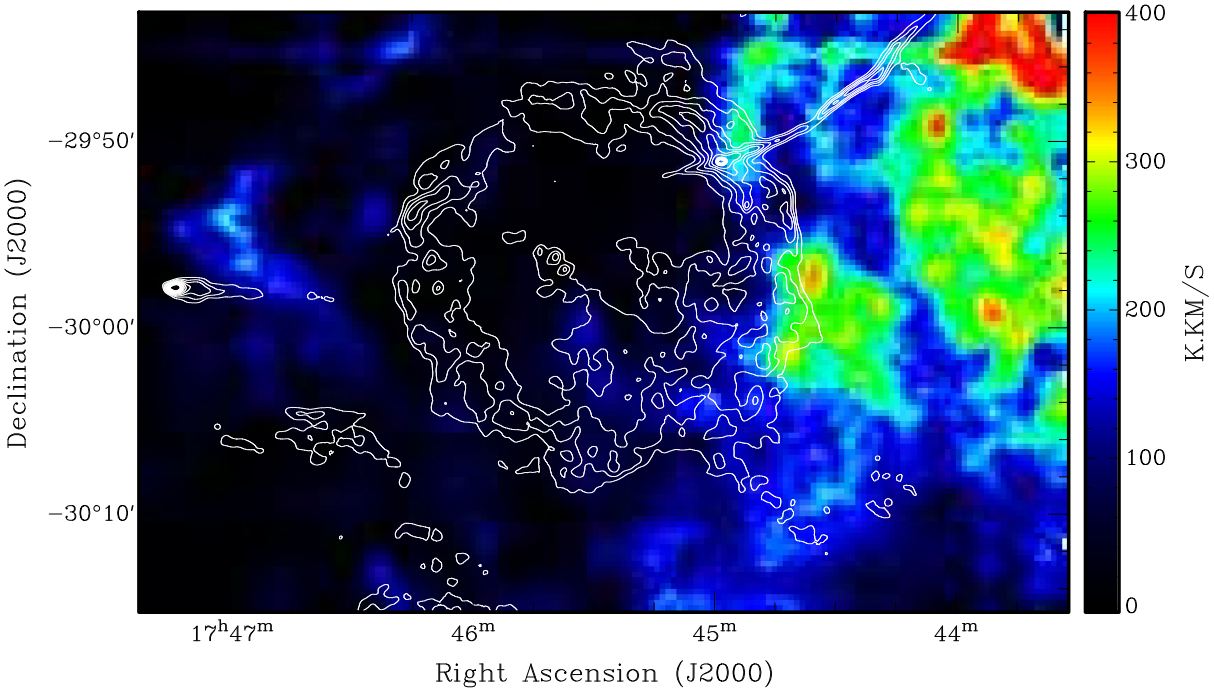

Figure 3. Distribution of ^{12}CO emission integrated between −178 and −60 km s^{-1}. The beam size is 53.6 arcsec × 53.6 arcsec. The colour scale is indicated at the right in units of K km s^{-1}. White contours at 0.0035, 0.008, 0.014, 0.019, and 0.025 mJy beam^{-1} represent the radio emission at 1.5 GHz.

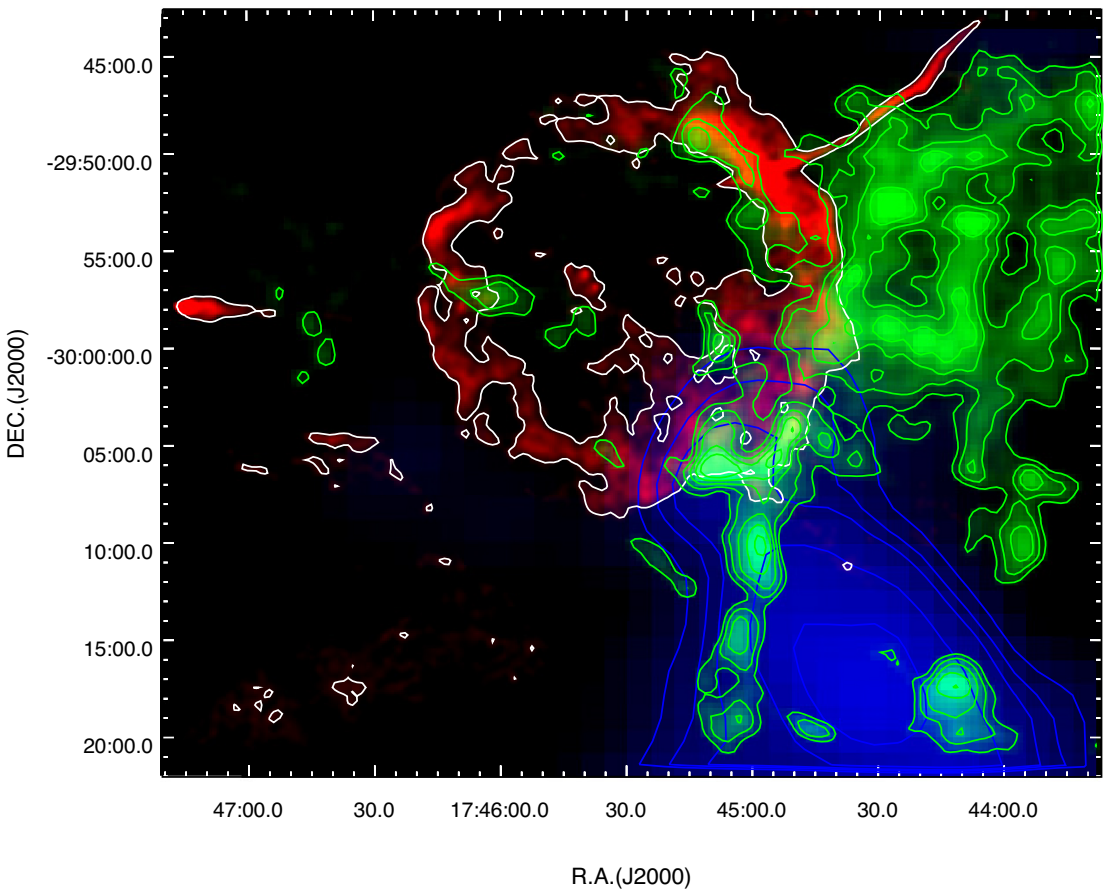

Figure 4. Composite RGB image of G359.1−0.5 and HESS J1745-303, where red is the radio emission at 1.5 GHz, green is the ^{12}CO emission (see Fig. 1), and blue is the TeV γ-ray emission observed with HESS, with blue contours overlaid. Radio continuum white contours at 0.008, 0.019, and 0.025 mJy beam^{-1} are also included.

et al. 2015), the total energy of cosmic ray protons accelerated in G359.1−0.5 can produce the observed the TeV emission (e.g. Hui et al. 2016). Therefore, several previous works have tried to explain HESS J1745-303 in terms of the SNR through the hadronic mechanism.

To explore the connection with molecular material, Aharonian et al. (2008) made use of a CO survey towards the Galactic Centre performed by Bitran et al. (1997) and obtained a map integrated between −100 and −60 km s^{-1}. We note that this survey is undersampled and has an half-power beamwidth (HPBW) of 8.8 arcmin, much larger than the 100 arcsec beam of the CO data in Uchida et al. (1992b). However, they have disregarded the fact that these velocities do not match those of the masers found around the SNR, and a cloud was found partially overlapping HESS J1745-303 from which the authors estimate that the interaction between G359.1−0.5 and a molecular cloud can account for the γ-rays emission in 'region A'.

Hayakawa et al. (2012) observed an area covering G359.1−0.5 and HESS J1745-303 in the CO J:2-1 line as part of the NANTEN2 Galactic-Center Survey. They detected the same cloud as Aharonian et al. (2008) but integrating in a wider velocity range, up to −15 km s^{-1}, and with a much better resolution (HPBW = 60 arcsec). The full area was also surveyed by de Wilt et al. (2017) in HC_3N, H_2O and several NH_3 transitions with the Mopra radio telescope and FWHM of ∼2 arcmin at a wavelength of 12 mm. Their maps are integrated between −200 and +200 km s^{-1} and show patchy molecular emission in the vicinity of the west–south side of G359.1−0.5. In particular, they report spectral broadening of more than 10 km s^{-1} at 'region A' (acknowledging that the kinematic velocities differ from the masers velocity by ∼50 km s^{-1}) and an enhanced ratio of NH_3 (3,3) over NH_3 (2,2), all indicative of heated gas. The authors attribute such heating to the passage of a shock front of unknown origin, since the clouds are outside the edge of the SNR.

Using the systematic velocity of the molecular gas associated with G359.1−0.5, based on the maser velocities, we produced an integrated CO image in Fig. 4 (see also Fig. 1). The velocity range encompassing this structure differs by at least 50 km s^{-1} from previous molecular studies towards HESS J1745-303, posing an utterly diverging picture when the new CO distribution and the TeV emission are compared. We observe in Fig. 4 an overlap between the southern tail of the CO structure, the SNR shell at the SW, and the northern end of HESS J1745-303. If we are to judge solely on morphological arguments, this spatial configuration could suggest that G359.1−0.5 is possibly triggering the observed γ-ray emission through hadronic interactions. However, there is no correlation between the CO distribution and the TeV intensity. On the contrary, the TeV peak appears to be surrounded, not overlapped, by a chain of molecular cloudlets.

In addition, we inspected the CO data cubes throughout the whole spectral ranges observed and found no positional coincidence between the CO emission and the γ-ray peak at any velocity. Moreover, the CO distribution unveils a minimum exactly coincident with the position of the TeV emission peak, as can be observed in the image integrated between −170 and +160 km s^{-1} displayed in Fig. 5. With the absence of a correlation between the CO and the

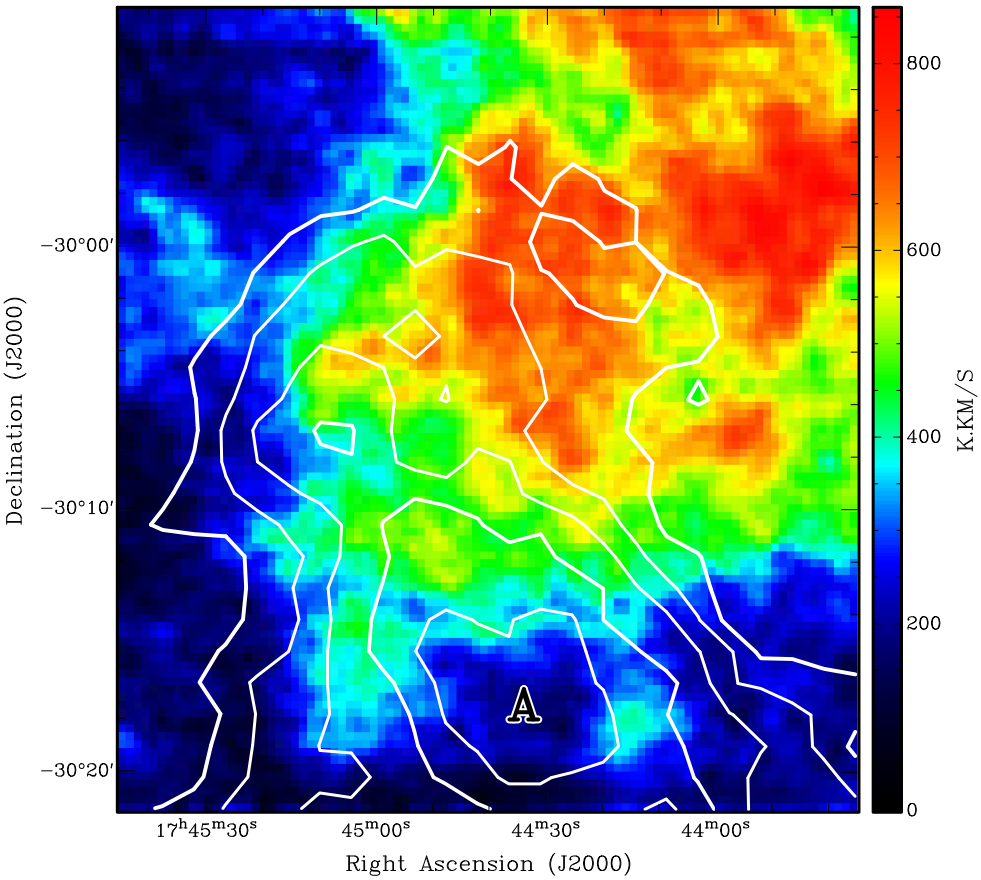

Figure 5. Distribution of the ^{12}CO emission in the vicinity of HESS J1745-303's region A integrated between −170 and +160 km seg^{-1}. The colour scale intensity is shown at the right. The TeV γ-ray emission is represented in white contours. The γ-ray peak A is coincident with a CO minimum.

γ-ray emission at any velocity from our data, the nature of HESS J1745-303 remains a mystery but can hardly be reconciled with a hadronic origin connected with G359.1−0.5.

5 CONCLUSIONS

We have carried out a molecular survey using the ^{12}CO and ^{13}CO J:1 − 0 lines towards the SNR G359.1−0.5. This study is complemented with archival HESS maps towards this region. The main findings can be summarized as follows:

(i) Four molecular clumps with densities $\sim 10^3$ cm^{-3}, some of them following closely the curvature of the remnant, have been detected in projection on to OH (1720 MHz) masers and at their same velocities.

(ii) On this basis, we identified a larger scale molecular structure between $v_{\rm LSR} = -12.48$ and $+1.86$ km s^{-1} extending to the west of G359.1−0.5. We propose that this structure, as well as the cloudlets associated with the OH (1720 MHz) masers, depicts the pre-shock molecular gas into which the SNR shock front is expanding.

(iii) We think it is highly unreliable that the ISM structures reported in the literature at velocities exceedingly different from those of the OH (1720 MHz) masers are related to the SNR.

(iv) The molecular cloud distribution at the masers velocities poorly matches the γ-ray distribution of HESS J1745-303. Thus, the γ-rays are unlikely to be directly related to the SNR. Inspection of our spectral data cubes at other velocities also does not show any molecular feature correlated with the intensity distribution of the γ-ray emission.

Future studies using molecular species tracers of high-density gas, like CS, C^{18}O, or H_2CO (Mangum & Wootten 1993; Bronfman, Nyman & May 1996), would be very helpful to identify shock signatures at possible interaction sites, particularly around masers D and E where no CO–maser correlation could be established.

ACKNOWLEDGEMENTS

LKE is supported by a CONICET fellowship. EMR, JAC, and JFAC are members of the Carrera del Investigador Científico of CONICET, Argentina. This research was partially funded by CONICET grants PIP 112-201207-00226 and 112-201701-00604. JAC and JFAC were supported by PIP 0102 (CONICET) and PICT-2017-2865 (ANPCyT). This work was also supported by the Agencia Estatal de Investigación grant AYA2016-76012-C3-3-P from the Spanish Ministerio de Economía y Competitividad (MINECO) and by the Consejería de Economía, Innovación, Ciencia y Empleo of Junta de Andalucía under research group FQM-322, as well as FEDER funds.

REFERENCES

Acero F. et al., 2015, ApJS, 218, 23
Aharonian F. et al., 2006, ApJ, 636, 777
Aharonian F. et al., 2008, A&A, 483, 509
Allen C. W., 1973, Astrophysical quantities. University of London, Athlone Press, London
Altenhoff W. J., Downes D., Pauls T., Schraml J., 1979, A&AS, 35, 23
Bamba A., Yokogawa J., Sakano M., Koyama K., 2000, PASJ, 52, 259
Bitran M., Alvarez H., Bronfman L., May J., Thaddeus P., 1997, A&AS, 125, 99
Brogan C. L. et al., 2013, ApJ, 771, 91
Bronfman L., Nyman L.-A., May J., 1996, A&AS, 115, 81
Chen B., Figueras F., Torra J., Jordi C., Luri X., Galadí-Enríquez D., 1999, A&A, 352, 459
de Wilt P., Rowell G., Walsh A. J., Burton M., Rathborne J., Fukui Y., Kawamura A., Aharonian F., 2017, MNRAS, 468, 2093
Dickman R. L., 1978, ApJS, 37, 407
Egger R., Sun X., 1998, in Breitschwerdt D., Freyberg M. J., Truemper J., eds, Lecture Notes in Physics, Vol. 506, IAU Colloq. 166: The Local Bubble and Beyond. Springer-Verlag, Berlin, p. 417
Elitzur M., 1976, ApJ, 203, 124
Frail D. A., Mitchell G. F., 1998, ApJ, 508, 690
Frail D. A., Goss W. M., Reynoso E. M., Giacani E. B., Green A. J., Otrupcek R., 1996, AJ, 111, 1651
Green A. J., Frail D. A., Goss W. M., Otrupcek R., 1997, AJ, 114, 2058
Hayakawa T., Torii K., Enokiya R., Amano T., Fukui Y., 2012, PASJ, 64, 8
Hewitt J. W., Yusef-Zadeh F., Wardle M., 2008, ApJ, 683, 189
Hui C. Y., Wu E. M. H., Wu J. H. K., Huang R. H. H., Cheng K. S., Tam P. H. T., Kong A. K. H., 2011, ApJ, 735, 115
Hui C. Y. et al., 2016, MNRAS, 457, 4262
Hunter S. D. et al., 1997, ApJ, 481, 205
Kalberla P. M. W., Burton W. B., Hartmann D., Arnal E. M., Bajaja E., Morras R., Poeppel W. G. L., 2005, VizieR Online Data Catalog, p. 8076
Koralesky B., Frail D. A., Goss W. M., Claussen M. J., Green A. J., 1998, AJ, 116, 1323
Kos J. et al., 2014, Science, 345, 791
Lazendic J. S., Wardle M., Burton M. G., Yusef-Zadeh F., Whiteoak J. B., Green A. J., Ashley M. C. B., 2002, MNRAS, 331, 537
Lockett P., Gauthier E., Elitzur M., 1999, ApJ, 511, 235
Mangum J. G., Wootten A., 1993, ApJS, 89, 123
Ohnishi T., Koyama K., Tsuru T. G., Masai K., Yamaguchi H., Ozawa M., 2011, PASJ, 63, 527
Qiao H.-H. et al., 2018, ApJS, 239, 15
Reed B. C., 2006, JRASC, 100, 146
Reich W., Fuerst E., 1984, A&AS, 57, 165
Reynoso E. M., Mangum J. G., 2000, ApJ, 545, 874
Reynoso E. M., Cichowolski S., Walsh A. J., 2017, MNRAS, 464, 3029
Rho J., Petre R., 1998, ApJ, 503, L167
Schlafly E. F., Finkbeiner D. P., 2011, ApJ, 737, 103
Truemper J., 1992, QJRAS, 33, 165
Truemper J., 1993, Science, 260, 1769
Turner B. E., 1982, ApJ, 255, L33
Uchida K., Morris M., Yusef-Zadeh F., 1992a, AJ, 104, 1533
Uchida K. I., Morris M., Bally J., Pound M., Yusef-Zadeh F., 1992b, ApJ, 398, 128
Wilson T. L., Rood R., 1994, ARA&A, 32, 191
Yusef-Zadeh F., Uchida K. I., Roberts D., 1995, Science, 270, 1801
Yusef-Zadeh F., Hewitt J. W., Cotton W., 2004, ApJS, 155, 421

This paper has been typeset from a TEX/LATEX file prepared by the author.